Dependence of enhanced asymmetry-induced transport on collision frequency

D. L. Eggleston
Occidental College, Physics Department, Los Angeles, California 90041, USA

(Received 23 May 2014; accepted 17 July 2014; published online 31 July 2014)

A single-particle code with collisional effects is used to study how asymmetry-induced radial transport in a non-neutral plasma depends on collision frequency. For asymmetries of the form $\phi_1(r)\cos(kz)\cos(\omega t - l\theta)$, two sources for the transport have been identified: resonant particles and axially trapped particles. The simulation shows that this latter type, which occurs near the radius where ω matches the azimuthal rotation frequency ω_R, is usually dominant at low collision frequency ν but becomes negligible at higher ν. This behavior can be understood by noting that axially trapped particles have a lower trapping frequency than resonant particles. In the low ν (banana) regime, the radial oscillations have amplitude $\Delta r \approx v_r/\omega_T$, so axially trapped particles dominate, and the transport may even exceed the resonant particle plateau regime level. As ν increases, collisions start to interrupt the slower axially trapped particle oscillations, while the resonant particles are still in the banana regime, so the axially trapped particle contribution to the transport decreases. At the largest ν values, axially trapped particle transport is negligible and the observed diffusion coefficient matches that given by plateau regime resonant particle theory. Heuristic models based on these considerations give reasonable agreement with the observed scaling laws for the value of the collision frequency where axially trapped particle transport starts to decrease and for the enhancement of the diffusion coefficient produced by axially trapped particles. © *2014 AIP Publishing LLC*. [http://dx.doi.org/10.1063/1.4891661]

I. INTRODUCTION

The cylindrical Malmberg-Penning non-neutral plasma trap is especially suited for basic studies of plasma transport since its excellent confinement can be perturbed and the resulting transport studied in a controlled manner. There have been many such experiments[1–11] that use non-axisymmetric electric or magnetic fields as the perturbation, but it has been difficult to explain the resulting asymmetry-induced transport theoretically. Early attempts to model this transport resulted in resonant particle (RP) transport theory,[12] but comparisons between this theory and experiments[7] do not show agreement. To determine the missing physics, we have previously studied[13,14] this asymmetry-induced transport using a single-particle computer code, including collisional effects. We found that for asymmetries of the form $\phi_1(r)\cos(kz)\cos(\omega t - l\theta)$, there are, in general, two sources for the transport: the previously mentioned resonant particles and another class of particles that are axially trapped in the asymmetry potential. These axially trapped particles (ATPs) often produced transport that was greatly enhanced over the level predicted by resonant particle theory. By varying the parameters of the code, we were able to find scaling laws characterizing this enhanced transport.

In this paper, we investigate the dependence of the enhanced transport on collision frequency. Interestingly, we find that the enhancement vanishes for large collision frequencies and the resulting transport is then given by the plateau regime of resonant particle transport theory. We show that this property, as well as one of the previously mentioned scaling laws, is rooted in the fact that the axially-trapped particles have a lower trapping frequency than the resonant particles.

II. SIMULATION METHODS

Complete details of our simulation methods are given in our previous paper[13] but are summarized here for convenience. Our code is constructed to model our experimental device which is shown in Fig. 1. Low density electrons are confined in the central region of length L between the negatively biased injection gate and dump gate. In order to maintain an azimuthal $E \times B$ drift comparable with a higher density plasma, a negatively biased wire is stretched along the axis of the device. The uniform axial magnetic field B providing radial confinement is strong enough so that the gyroradius is much smaller than the wall radius R. The walls of the confinement region are divided into 40 sectors (five axial divisions S1–S5 with eight azimuthal divisions each) which allows application of an asymmetric electric field. The voltages applied to these sectors are typically chosen so that the field consists primarily of a single Fourier mode. The remaining details of the experiment are given elsewhere.[7]

The code follows the dynamics of single particles in prescribed fields; inter-particle fields are not included. The prescribed fields are set by the center wire potential and the asymmetric potential. The center wire potential is given by

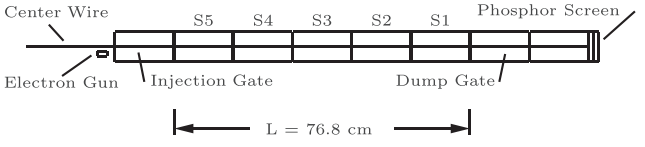

FIG. 1. Schematic of the Occidental College trap. The usual plasma column is replaced by a biased wire to produce the basic dynamical motions in low density electrons injected from an off-axis gun.

$$\phi_0(r) = \phi_{cw}\frac{\ln(R/r)}{\ln(R/a)}, \tag{1}$$

where ϕ_{cw} is the bias of the center wire, R is the radius of the wall, and a is the radius of the center wire. The asymmetric potential is chosen to be either a helical wave

$$\phi_{hel}(r,\theta,z,t) = \phi_1(r)\cos(kz - l\theta + \omega t) \tag{2}$$

or an axially standing wave

$$\phi_{sw}(r,\theta,z,t) = 2\phi_1(r)\cos(kz)\cos(-l\theta + \omega t). \tag{3}$$

In Eqs. (2) and (3), $k = n\pi/L$ and n is the axial wavenumber, l is the azimuthal wavenumber, ω is the asymmetry frequency, and z is the measured from one end of the confinement region. The amplitude $\phi_1(r)$ is taken to be of the form $\phi_{10}(r/R)^l$, where ϕ_{10} is a constant. This form closely approximates the exact vacuum solution.

The particle motions in the code are governed by

$$\frac{dr}{dt} = v_r, \quad r\frac{d\theta}{dt} = v_\theta, \quad \frac{dz}{dt} = v_z, \quad \frac{dv_z}{dt} = \frac{qE_z}{m} - \nu v_z, \tag{4}$$

where ν is the electron-electron collision frequency. For typical experimental conditions, the gyroradius is much smaller than the wall radius R and the cyclotron frequency is much larger than all other dynamical frequencies. We thus ignore the cyclotron motion and follow the motion of the guiding center. In this drift approximation, v_r and v_θ are given by

$$v_r = \frac{E_\theta}{B}, \quad v_\theta = -\frac{E_r}{B}. \tag{5}$$

The electric fields are obtained from the prescribed potentials: $E_r = -\frac{\partial\phi}{\partial r}$, $E_\theta = -\frac{1}{r}\frac{\partial\phi}{\partial\theta}$, and $E_z = -\frac{\partial\phi}{\partial z}$. The zeroth order variation of E_r defines the azimuthal rotation frequency ω_R

$$\omega_R = -\frac{E_{r0}}{rB} = \frac{-\phi_{cw}}{r^2 B\ln(R/a)}, \tag{6}$$

where in the last step, we have used Eq. (1). Since ϕ_{cw} is typically negative, ω_R is positive.

Equations (4) and (5) are solved using a fourth-order Runge-Kutta method.[15] In addition to the collisional drag term, νv_z in Eq. (4), a random velocity step is added to v_z after each time increment, in accordance with the Langevin prescription.[13,16,17] Parameters are chosen to match our typical experimental conditions and unless otherwise specified are $B = 364\,\text{G}$, $L = 76.8\,\text{cm}$, $R = 3.87\,\text{cm}$, $a = 0.007$ in, $kT = 4\,\text{eV}$, $\phi_{10} = 0.1\,\text{V}$, and $n = l = 1$. Initially, all particles are placed at the same radius but are distributed in z, θ, and v_z. To account for the variation in particle density in a Maxwellian velocity distribution, the particles are assigned a weighting factor $W_i = \exp[-(v_{zi}/v_{th})^2]$, where v_{th} is the thermal velocity and i is the particle number index. Particles reaching the ends of the trap are treated by applying one of two options, periodic boundaries or specular reflection. The simulation is run long enough to insure that transient behavior has settled, typically $\nu T \approx 1$, where T is the total run time.

The transport is characterized by calculating the diffusion coefficient. This is given by

$$D = \frac{1}{2}\frac{d}{dt}[\langle(\Delta r)^2\rangle - \langle\Delta r\rangle^2], \tag{7}$$

where

$$\langle\Delta r\rangle \equiv \frac{1}{W}\sum_{i=1}^{M} W_i\left[r_i(t) - r_i(0)\right] \tag{8}$$

and

$$\langle(\Delta r)^2\rangle \equiv \frac{1}{W}\sum_{i=1}^{M} W_i\left[r_i(t) - r_i(0)\right]^2. \tag{9}$$

Here, M is the total number of particles (typically 64 k) and $W = \sum W_i$ is the sum over weighting factors.

III. THEORETICAL BACKGROUND

One approach to modeling asymmetry-induced transport is to use resonant particle theory.[12] In this approach, the asymmetric potential $\phi_1(r,\theta,z,t)$ is decomposed into Fourier modes of amplitude $\phi_{nl\omega}(r)$ and characterized by axial mode n, azimuthal mode l, and angular frequency ω:

$$\phi_1(r,\theta,z,t) = \sum_{n,l,\omega}\phi_{nl\omega}(r)\cdot\exp\left[i\left(\frac{n\pi}{L}z + l\theta - \omega t\right)\right]. \tag{10}$$

The transport is then calculated for each mode and the total flux found by summing these contributions. The theory shows that the transport for each mode is dominated by particles with velocities that cause them to move in resonance with the mode. This resonant velocity is given by

$$v_{res} = \frac{L}{n\pi}(\omega - l\omega_R). \tag{11}$$

In our previous paper,[13] we found that our simulation results agreed with resonant particle theory for a simple helical asymmetry of the form found in Eq. (2), but for the more experimentally relevant case of the standing wave asymmetry (Eq. (3)), the results are more nuanced. Such an asymmetry can be written as the sum of two counter-propagating helical asymmetries with oppositely signed n values:

$$\phi_{sw}(r,\theta,z,t) = \phi_1(r)\left[\cos\left(\frac{n\pi}{L}z - l\theta + \omega t\right) + \cos\left(\frac{-n\pi}{L}z - l\theta + \omega t\right)\right]. \tag{12}$$

From Eq. (11), we see that these two terms have resonant velocities of equal magnitude but opposite signs. As long as these two velocities are well separated, the simulation and resonant particle theory agree. However, at radii where the asymmetry frequency ω matches $l\omega_R$, both resonant velocities are zero. In this case, the mode resonance structures overlap and resonant particle theory is no longer valid. For

lower values of collisionality, the simulation here typically gives a level of transport that is much larger than predicted by resonant particle theory. Here, the transport is dominated by particles with velocities low enough to be axially trapped at one end of the machine by the asymmetry potential. These particles have larger radial excursions than the resonant particles and thus produce an enhancement of the transport.

To characterize this enhancement, it is useful to compare the diffusion coefficient D_{sw} obtained when running the simulation using a standing wave asymmetry with the value $2D_{hel}$, where D_{hel} is the diffusion coefficient obtained when running the simulation using a single helical asymmetry. The factor of two is appropriate since each of the constituent helical waves in a standing wave produces the same value of D. Thus, $2D_{hel}$ represents the value we expect from the simulation if resonant particle theory is correct.

IV. RESULTS

Since our focus here is characterizing how the enhanced transport depends on collision frequency, we set the asymmetry frequency to the value $\omega_1 \approx \omega_R$ that gives the maximum value of D for the standing wave asymmetry. In Fig. 2, we show how this diffusion coefficient varies with collision frequency ν for three representative sets of parameters that give varying levels of enhancement. In Fig. 2(a) we choose a scaled radius $r/R = 0.9$ and a center wire bias $\phi_{cw} = -20\,\mathrm{V}$. In accordance with the parameter scaling found in Ref. 13 and discussed in Sec. V, these parameters give a large enhancement. In Fig. 2(b), we keep r/R the same and change ϕ_{cw} to $-80\,\mathrm{V}$, yielding a smaller enhancement. Finally, in Fig. 2(c), we hold ϕ_{cw} at $-80\,\mathrm{V}$ and decrease r/R to 0.5. This gives the smallest enhancement, again in line with expectation from the parameter scaling. The solid circles in the figure give the values obtained for a standing wave asymmetry while the open circles show the result of doubling the values obtained for a helical asymmetry. In each case, the standing wave asymmetry gives, for the lower values of the collision frequency, a diffusion coefficient D_{sw} that is larger than the value $2D_{hel}$ expected if resonant particle theory was applicable. As ν is increased, however, this enhancement vanishes and we obtain $D_{sw} = 2D_{hel}$. The lines in the plots show the predictions of resonant particle theory[12] for the banana and plateau regimes and show that these predictions track the simulation values $2D_{hel}$. The roughly factor of two difference between $2D_{hel}$ and $2D_{Ban}$ we ascribe to the heuristic nature of the banana regime theory.

Several features of these graphs are worth noting. Firstly, note that the amount of transport enhancement at low values of ν is different for each case shown. Indeed, the dependence of the enhancement on radius and center wire bias was shown in our previous work[13] to follow an empirical scaling $D_{net}/2D_{hel} = 750(r/R)^{3.86}/|\phi_{cw}|^{0.87}$, where ϕ_{cw} is in volts and $D_{net} = D_{sw} - 2D_{hel}$ is the amount of enhancement. Secondly, note that, at low values of ν, both D_{sw} and $2D_{hel}$ increase with the first power of ν, which is typical of banana regime transport models. Thirdly, note that, when the enhancement is large (cf. Figs. 2(a) and 2(b)), D_{sw} may exceed the level given by resonant particle plateau regime theory but then decreases with higher values of ν. In all cases, D_{sw} becomes equal to $2D_{hel}$ at the highest values of ν. Lastly, the value of ν at which D_{net} starts to decrease also differs for each case shown. In Fig. 3, we plot this breakpoint collision frequency ν_{bp} (estimated by examining plots of D_{net} versus ν for various parameters) versus the trapping frequency for axially trapped particles ω_T^{ATP} (defined in Sec. V). The trend line indicates a simple relationship between these quantities.

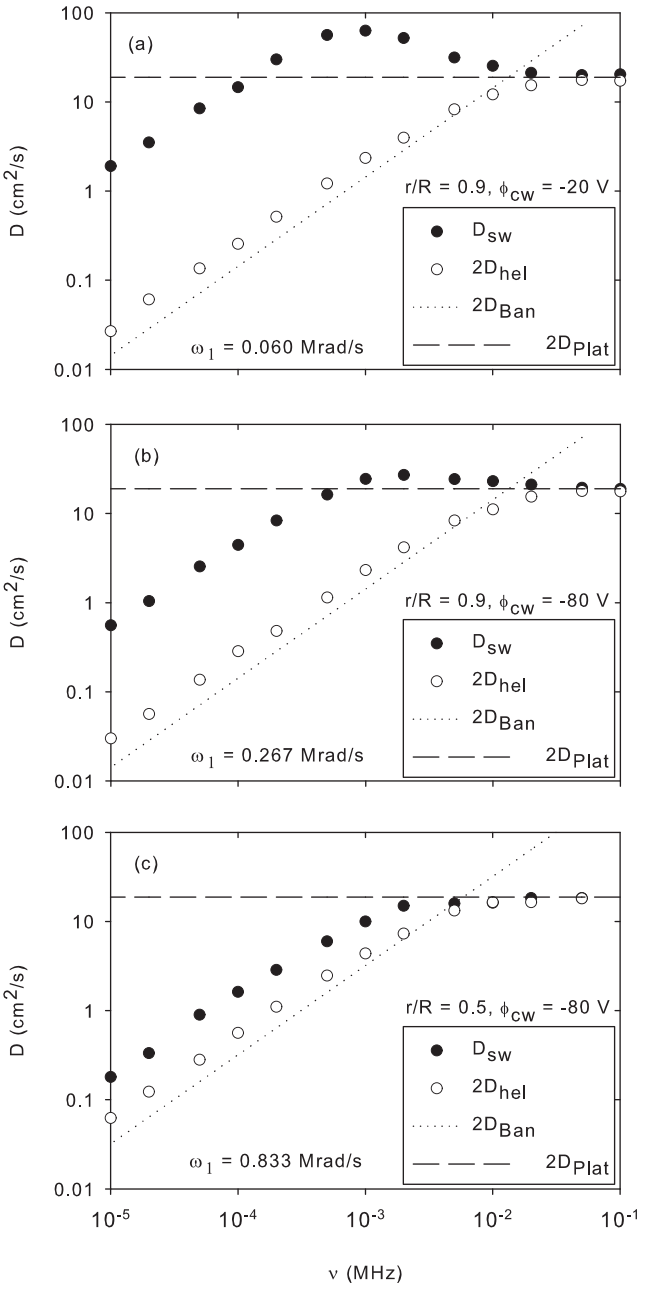

FIG. 2. Diffusion coefficient D obtained from the simulation versus collision frequency ν for three representative sets of parameters giving varying levels of enhancement. The solid circles show the results when a standing wave asymmetry is used. The open circles show the diffusion coefficient for a helical asymmetry doubled which should be equivalent to the standing wave case according to resonant particle theory. The dotted and dashed lines show the analytical results of resonant particle theory for the banana and plateau regimes, respectively. (a) Results for scaled radius $r/R = 0.9$ and center wire bias $\phi_{cw} = -20\,\mathrm{V}$. (b) Results for $r/R = 0.9$ and $\phi_{cw} = -80\,\mathrm{V}$. (c) Results for $r/R = 0.5$ and $\phi_{cw} = -80\,\mathrm{V}$.

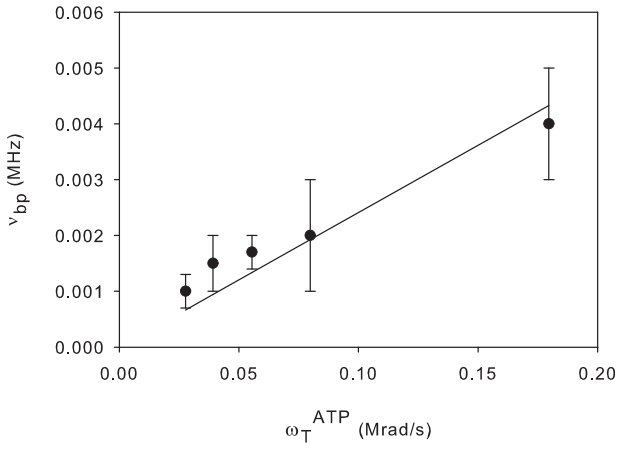

FIG. 3. Breakpoint collision frequency ν_{bp} versus the trapping frequency for axially trapped particles ω_T^{ATP}. We define ν_{bp} as the collision frequency at which the transport enhancement $D_{net} = D_{sw} - 2D_{hel}$ starts to decrease. The error bars give the uncertainty in determining this value from the limited simulation data. The line is the best fit to the data passing through the origin and has slope 0.024.

V. DISCUSSION

The noted features of these graphs can be understood through the following considerations. In the absence of collisions, RPs in a helical asymmetry undergo trapped particle oscillations at angular frequency[12]

$$\omega_T^{RP} = \sqrt{\left(\frac{e}{m}k^2 - \frac{l^2}{rB}\frac{d\omega_R}{dr}\right)\phi_1}, \tag{13}$$

whereas for ATPs in a standing wave asymmetry, the frequency is (see Appendix)

$$\omega_T^{ATP} = \sqrt{-\frac{l^2}{rB}\frac{d\omega_R}{dr}2\phi_1}. \tag{14}$$

For the parameters of our simulation, the first term in Eq. (13) dominates the second for all but small radii, so typically $\omega_T^{RP} > \omega_T^{ATP}$. For both types of trapped particles, the radial excursion during oscillation is $\Delta r \approx v_r/\omega_T$, where v_r is the radial $E \times B$ drift due to the asymmetry (see Eq. (5)) and ω_T is the relevant trapping frequency. Since $\omega_T^{RP} > \omega_T^{ATP}$, the radial steps for axially trapped particles are larger than those for resonant particles and, other things being equal, $D_{sw} > 2D_{hel}$. This gives a qualitative explanation for the enhanced transport observed for a standing wave asymmetry at low values of ν.

The relative size of ω_T^{RP} and ω_T^{ATP} also explains the general shape of the curves in Fig. 2. Generally, the banana transport regime ends when the collision frequency is high enough to interrupt the trapping oscillations. Since $\omega_T^{ATP} < \omega_T^{RP}$, the enhanced transport should end at a value of the collision frequency less than the one where the resonant particle banana regime transitions to the plateau regime (where the dotted and dashed lines in Fig. 2 intersect). This prediction is consistent with the simulation results shown in Fig. 2.

These models can be made more quantitative by noting that the relevant collision frequency is not our simulation parameter ν but a higher value ν_{eff}. This reflects the fact that

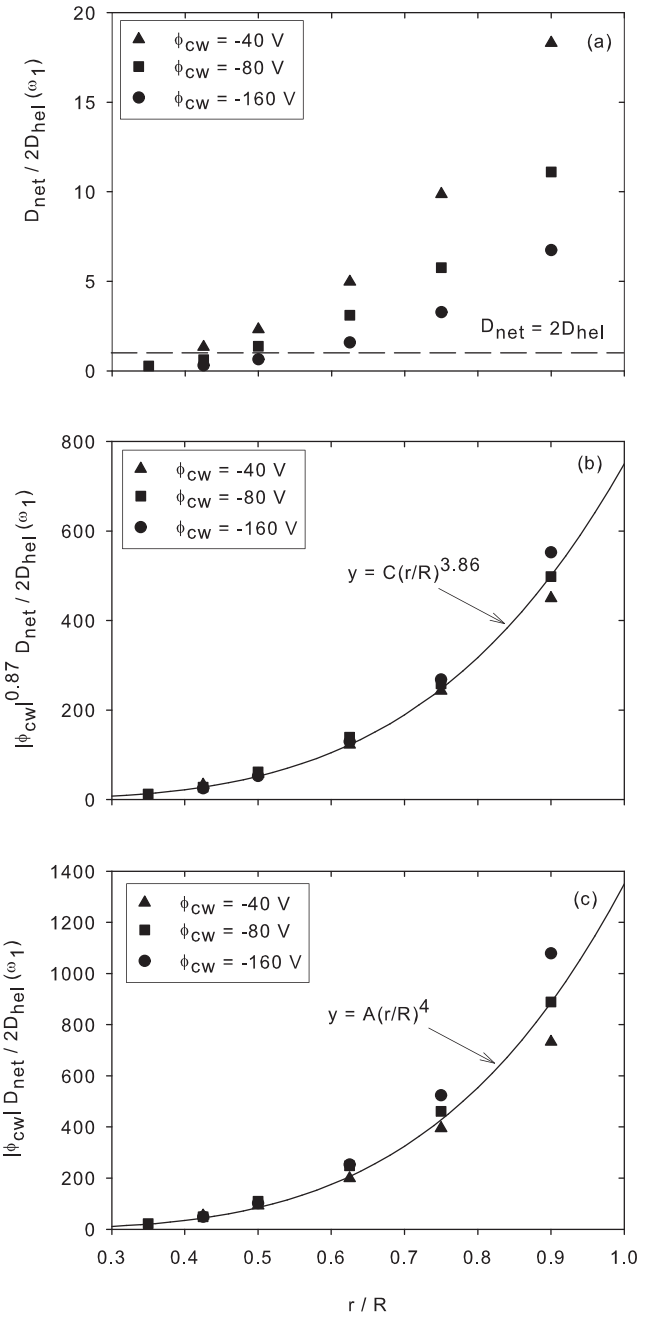

FIG. 4. Variation of $D_{net}/2D_{hel}$ with scaled radius r/R and center wire bias ϕ_{cw} for $\nu = 10^{-3}$ MHz. Plot (a) shows the raw data and plot (b) shows the best empirical scaling of the data. Here, the constant C = 750. Plot (c) shows the result of plotting the data using the scaling obtained from our heuristic model (cf. Eq. (17)). Here, A = 1350.

only a relatively small velocity scattering is required to move a particle from trapped to passing populations, whereas ν is the 90° scattering frequency. Here, we employ the usual[12] heuristic estimate $\nu_{eff} \approx \nu(\bar{v}/\Delta v)^2$, where $\bar{v}$ is the thermal velocity and Δv is the velocity change required to move the particle from trapped to passing. Our model is that the transport due to axially trapped particles will start to decrease when these effective collisions interrupt the trapping oscillations. We express this as $\omega_T^{ATP}\tau \approx \pi$, where $\tau = 1/\nu_{eff}^{ATP}$. Using the heuristic expression for ν_{eff}^{ATP} and estimating $\frac{1}{2}m(\Delta v^{ATP})^2 = 2q\phi_1$ as the energy needed to change an axially trapped particle to a passing particle, we obtain

$$\nu_{bp} = \left(\frac{\Delta v}{\bar{v}}\right)^2 \frac{\omega_T^{ATP}}{2\pi} \approx 0.032\,\omega_T^{ATP}. \tag{15}$$

The scaling with ω_T^{ATP} matches that found in Fig. 3 and the agreement in the numerical factor (0.024 compared with 0.032 for our model) is acceptable considering the heuristic nature of our model.

We can also make our model of the transport enhancement more quantitative by employing the usual heuristic expression for the radial diffusion coefficient $D = F\nu_{\text{eff}}(\Delta r)^2$, where Δr is the step size of the random walk, ν_{eff} is the rate at which steps are taken, and F is the fraction of particles participating. For low collision frequencies, we characterize the amount of enhancement the standing wave asymmetry produces by $D_{net}/2D_{hel}$, where $D_{net} = D_{sw} - 2D_{hel}$. In our previous paper,[13] we obtained the data shown in Fig. 4(a) and the empirical scaling shown in Fig. 4(b). We now apply our simple model in an attempt to explain this scaling. Applying the heuristic expression for D, we obtain

$$\frac{D_{net}}{2D_{hel}} = \frac{D_{sw}}{2D_{hel}} - 1 = \frac{F^{ATP}\nu_{eff}^{ATP}\left(\frac{v_r^{ATP}}{\omega_T^{ATP}}\right)^2}{2F^{RP}\nu_{eff}^{RP}\left(\frac{v_r^{RP}}{\omega_T^{RP}}\right)^2} - 1, \tag{16}$$

whereas before, the superscripts ATP and RP specify quantities for axially trapped particles and resonant particles, respectively. The two expressions for trapping frequency are given by Eqs. (13) and (14). The ratio $v_r^{ATP}/v_r^{RP} = 2$. We again use the heuristic expressions for ν_{eff} and take $\Delta v^{RP} = \omega_T^{RP}/k$ from resonant particle theory.[12] Finally, we estimate the ratio $F^{ATP}/F^{RP} \approx 1/3$. This stems from the fact that axially trapped particles occupy a smaller fraction of possible z and θ values than resonant particles. For the radii considered here, the first terms in Eqs. (13) and (16) dominate the second. Inserting parameter values, we obtain for our model

$$\frac{D_{net}}{2D_{hel}} \approx 2000\frac{(r/R)^4}{|\phi_{cw}|}, \tag{17}$$

where ϕ_{cw} is in volts. The scaling with r/R and ϕ_{cw} is close to the best fit empirical scaling $(r/R)^{3.86}/|\phi_{cw}|^{0.87}$. As shown in Fig. 4(c), if we force the scaling of our model on the simulation results, the fit to the data is still good, with the agreement in numerical factors (1350 compared with 2000 for our model) acceptable considering the heuristic nature of the model.

VI. CONCLUSION

We have presented results from a simple particle simulation of radial transport in our non-neutral plasma device. The results show that the diffusion coefficient for a standing wave asymmetry is larger than predicted from resonant particle theory for low values of the collision frequency but matches the theory for high values. We have shown that these results can be understood by noting the difference in trapping frequency for axially trapped particles and resonant particles. Our heuristic models for the breakpoint collision frequency and transport enhancement give parameter scalings and numerical values in reasonable agreement with the simulation results.

ACKNOWLEDGMENTS

This material is based upon work supported by the Department of Energy under Award No. DE-FG02-06ER54882 and National Science Foundation Grant No. PHY-1003952.

APPENDIX: TRAPPING FREQUENCY FOR AXIALLY TRAPPED PARTICLES

We consider a total potential consisting of the potential produced by the biased center wire plus the standing wave asymmetry potential

$$\phi(r,\theta,z,t) = \phi_0(r) + 2\phi_1(r)\cos kz\cos(\omega t - l\theta), \tag{A1}$$

where $\phi_0(r)$ is given by Eq. (1). In the drift approximation, we then have

$$\frac{dr}{dt} = \frac{E_\theta}{B} = -\frac{2l\phi_1(r)}{rB}\cos kz\sin\eta, \tag{A2}$$

$$\frac{d\theta}{dt} = \frac{v_\theta}{r} = \omega_R(r) + \frac{2}{rB}\frac{d\phi_1(r)}{dr}\cos kz\cos\eta, \tag{A3}$$

and

$$\frac{dv_z}{dt} = -\frac{2ek}{m}\phi_1(r)\sin kz\cos\eta, \tag{A4}$$

where $\eta = \omega t - l\theta$ and $\omega_R(r) = \frac{1}{rB}\frac{d\phi_0}{dr}$ is the azimuthal $E\times B$ rotation frequency.

We are interested in the behavior of particles trapped in the asymmetric potential. We choose to consider oscillations in the quantity η since this will also give the oscillation frequency of r and v_z through Eqs. (A2) and (A4), respectively. Forming $\frac{d^2\eta}{dt^2}$, we obtain

$$\begin{aligned}\frac{d^2\eta}{dt^2} = -l\Bigg[&\frac{dr}{dt}\frac{d\omega_R}{dr} - \frac{2}{B}\left(\frac{1}{r^2}\frac{dr}{dt}\frac{d\phi_1}{dr}\cos kz\cos\eta\right.\\ &-\frac{1}{r}\frac{dr}{dt}\frac{d^2\phi_1}{dr^2}\cos kz\cos\eta + \frac{k}{r}\frac{d\phi_1}{dr}\frac{dz}{dt}\sin kz\cos\eta\\ &\left.+\frac{1}{r}\frac{d\phi_1}{dr}\left(\omega - l\frac{d\theta}{dt}\right)\cos kz\sin\eta\right)\Bigg].\end{aligned} \tag{A5}$$

Using Eqs. (A2) and (A3) and dropping terms that are second order in the perturbing potential ϕ_1, we obtain

$$\begin{aligned}\frac{d^2\eta}{dt^2} = \frac{2l}{rB}\Bigg[&l\phi_1\frac{d\omega_R}{dr}\cos kz\sin\eta + \frac{d\phi_1}{dr}kv_z\sin kz\cos\eta\\ &+\frac{d\phi_1}{dr}(\omega - l\omega_R)\cos kz\sin\eta\Bigg].\end{aligned} \tag{A6}$$

We now use the fact that we are interested in axially trapped particles. These occur for low velocities and near the radius where $\omega \approx l\omega_R$ so the second and third terms of Eq. (A6) drop out. We are left with

$$\frac{d^2\eta}{dt^2} = -\omega_T^2 \sin\eta, \tag{A7}$$

where

$$\omega_T^2 = -\frac{l^2}{rB}\frac{d\omega_R}{dr}2\phi_1. \tag{A8}$$

Since $d\omega_R/dr$ is negative, ω_T is positive. Equation (A7) is the well known pendulum equation with ω_T being the small angle oscillation frequency. In this context, this is the oscillation frequency of particles deeply trapped in the asymmetry potential.

[1]D. L. Eggleston, T. M. O'Neil, and J. H. Malmberg, Phys. Rev. Lett. **53**, 982 (1984).
[2]J. Notte and J. Fajans, Phys. Plasmas **1**, 1123 (1994).
[3]X.-P. Huang, F. Anderegg, E. M. Hollman, C. F. Driscoll, and T. M. O'Neil, Phys. Rev. Lett. **78**, 875 (1997).
[4]J. M. Kriesel and C. F. Driscoll, Phys. Rev. Lett. **85**, 2510 (2000).
[5]D. L. Eggleston and B. Carrillo, Phys. Plasmas **9**, 786 (2002).
[6]E. Gilson and J. Fajans, Phys. Rev. Lett. **90**, 015001 (2003).
[7]D. L. Eggleston and B. Carrillo, Phys. Plasmas **10**, 1308 (2003).
[8]A. A. Kabantsev, J. H. Yu, R. B. Lynch, and C. F. Driscoll, Phys. Plasmas **10**, 1628 (2003).
[9]J. R. Danielson and C. M. Surko, Phys. Plasmas **13**, 055706 (2006).
[10]Y. Soga, Y. Kiwamoto, and N. Hashizume, Phys. Plasmas **13**, 052105 (2006).
[11]A. A. Kabantsev, Daniel H. E. Dubin, C. F. Driscoll, and Yu. A. Tsidulko, Phys. Rev. Lett. **105**, 205001 (2010).
[12]D. L. Eggleston and T. M. O'Neil, Phys. Plasmas **6**, 2699 (1999).
[13]D. L. Eggleston, Phys. Plasmas **19**, 042307 (2012).
[14]D. L. Eggleston, Phys. Plasmas **14**, 012302 (2007).
[15]R. Hornbeck, *Numerical Methods* (Quantum, New York, 1975), pp. 194–196.
[16]D. H. E. Dubin, Phys. Plasmas **15**, 072112 (2008).
[17]F. Reif, *Fundamentals of Statistical and Thermal Physics* (McGraw-Hill, New York, 1965), pp. 560–575.